

Supporting Information

Concave Silica Nanosphere with a Functionalized Open-Mouthed Cavity as Highly Active and Durable Catalytic Nanoreactor

Jin Goo Kim,^{†,‡,§} Amit Kumar,^{†,‡,§} Seung Jin Lee,^{†,‡} Junghoon Kim,[‡] Dong-Gyu Lee,^{†,‡} Taewan Kwon,^{†,‡} Seung Hwan Cho,[‡] and In Su Lee^{*,†,‡}

[†]National Creative Research Initiative Center for Nanospace-confined Chemical Reactions (NCCRs) and

[‡]Department of Chemistry, Pohang University of Science and Technology (POSTECH), Pohang 37673, Korea

*To whom correspondence should be addressed

e-mail: insulee97@postech.ac.kr (I. S. L.)

[§]These authors contributed equally to this work and both should be considered as the first author.

X-ray Photoelectron Spectroscopy (XPS): XPS measurements were performed on a PHI versaprobe system, using a monochromatic Al K α source. High-resolution narrow scans were performed at constant pass energy of 58.7 eV and steps of 0.1 eV. The photoelectrons were detected at a takeoff angle of $\Phi = 45^\circ$ with respect to the surface normal. The pressure in the analysis chamber was maintained below 2.4×10^{-9} Torr for data acquisition. The data were converted to VAMAS format and processed using Multipak software. The binding energy (BE) scale was internally referenced to the C 1s peak (BE for C–C = 284.8 eV).

Brunauer–Emmett–Teller (BET) Surface Properties Measurements: N₂ adsorption–desorption analysis was carried out using a Micromeritics ASAP 2020 at Korea Basic Science Institute (Dr. Sang Moon Lee). The typical sample weight used was 50–100 mg. The outgas condition was set to 100 °C under vacuum for overnight, and all adsorption–desorption measurements were carried out at liquid nitrogen temperature (–196 °C). The original DFT method for the slit pore geometry was used to extract the pore size distribution from the adsorption branch using the Micromeritics software.^{1–4} A Horvath-Kawazoe method was used to extract the microporosity.⁵ Barret-Joyner-Halenda model (BJH) method was used to extract the mesoprosity.⁶

X-Ray Diffraction (XRD) Analysis: Powder X-ray diffraction patterns were obtained using an X-ray diffractometer (18 kW, Rigaku, Japan).

(1) Balbuena, P. B.; Gubbins, K. E. Classification of adsorption behavior: simple fluids in pores of slit-shaped geometry, *Fluid Phase Equilibria* **1992**, 76, 21–35.

(2) Olivier, J. P. Modeling physical adsorption on porous and nonporous solids using density functional theory, *J. Porous Mater.* **1995**, 2, 9–17.

(3) Maddox, M. W.; Olivier, J. P.; Gubbins, K. E. Characterization of MCM-41 using molecular simulation: Heterogeneity effects, *Langmuir* **1997**, 13, 1737–1745.

(4) Olivier, J. P. Improving the models used for calculating the size distribution of micropore volume of activated carbons from adsorption data, *Carbon* **1998**, 36, 1469–1472.

(5) Horvath, G.; Kawazoe, K. Method for the calculation of effective pore size distribution in molecular sieve carbon, *J. Chem. Eng. Jpn.* **1983**, 16, 470–475.

(6) Barrett, E. P.; Joyner, L.G.; Halenda, P.P. The determination of pore volume and area distributions in porous substances. I. Computations from Nitrogen Isotherms, *J. Am. Chem. Soc.* **1951**, 73, 373–380.

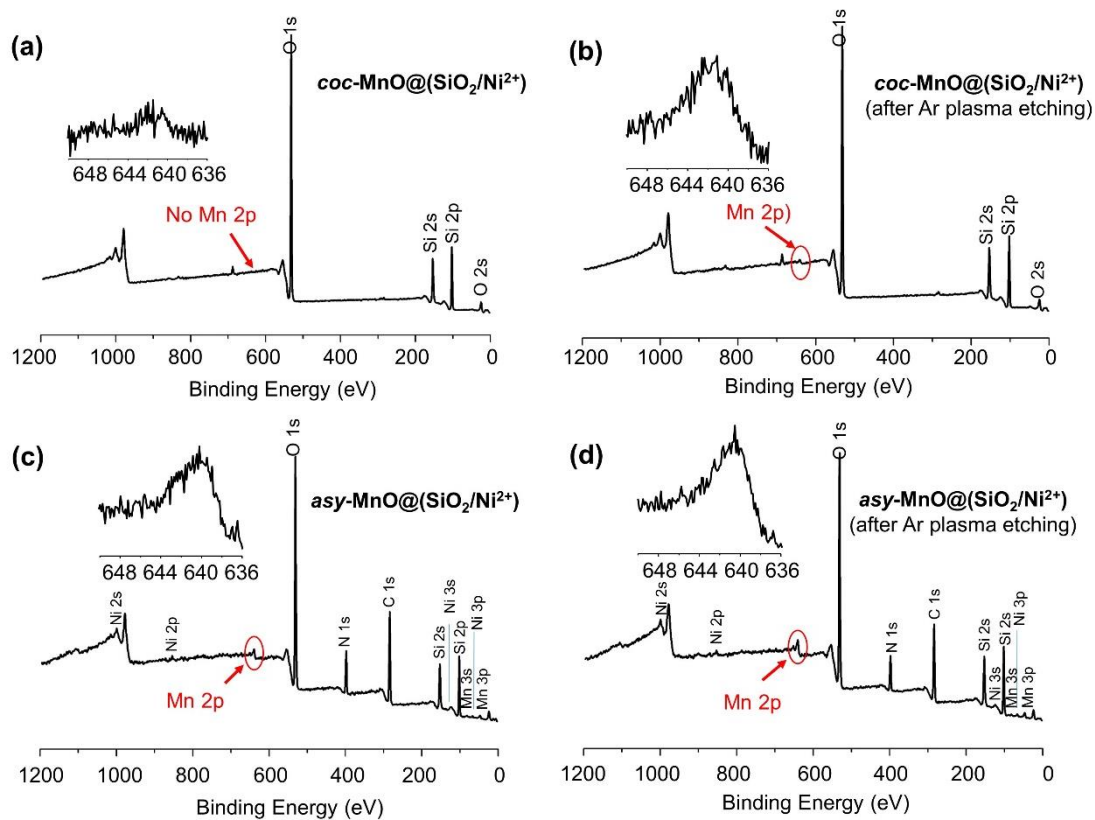


Figure S1. XPS analysis of *coc*-MnO@(SiO₂/Ni²⁺) and *asy*-MnO@(SiO₂/Ni²⁺) before and after Ar plasma etching. Graphs shown in the insets represent high resolution Mn 2p profiling.

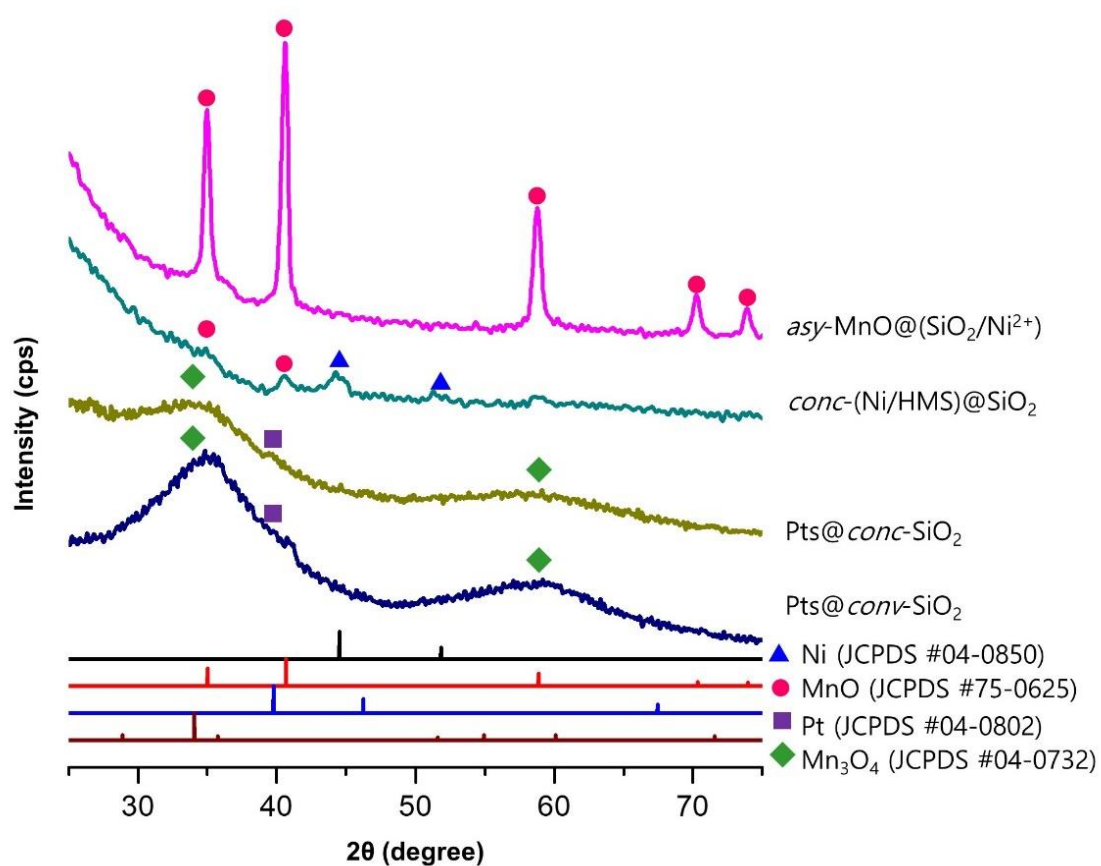


Figure S2. XRD patterns of *asy*-MnO@(SiO₂/Ni²⁺), *conc*-(Ni/HMS)@SiO₂, Pt@*conc*-SiO₂ and Pt@*conv*-SiO₂ and their comparison with standard data.

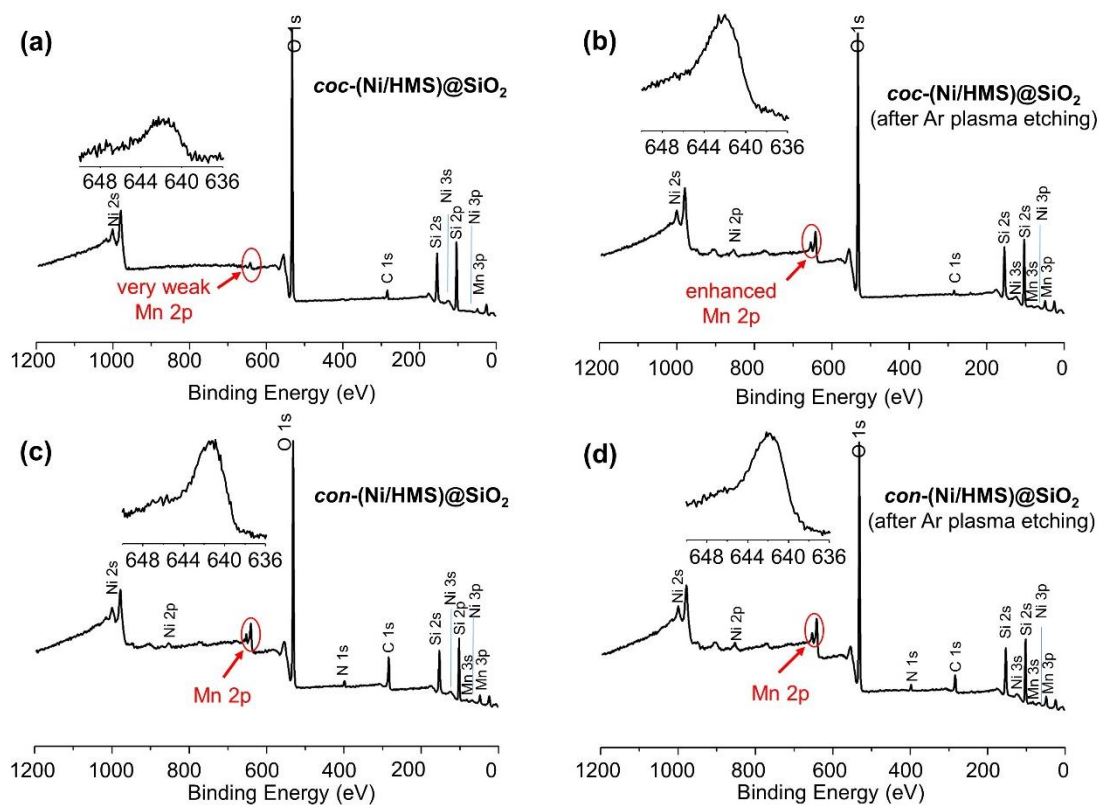


Figure S3. XPS analysis of coc-(Ni/HMS)@SiO₂ and conc-(Ni/HMS)@SiO₂ before and after Ar plasma etching. Graphs shown in the insets represent high resolution Mn 2p profiling.

Nanoparticles	S_{BET} (m^2g^{-1})	S_{ext} (cm^3g^{-1})	V_{mic} (cm^3g^{-1})	V_{tot} (cm^3g^{-1})	D_{ave} (nm)	$D_{\text{BJH Ad}}$ (nm)	$D_{\text{BJH De}}$ (nm)
<i>conc</i>-(Ni/HMS)@SiO₂	44.5	20.2	0.01	0.27	24.48	42.16	30.03
<i>coc</i>-(Ni/HMS)@SiO₂	91.0	64.2	0.01	0.57	25.03	33.21	24.01

S_{BET} =specific surface area(Brunauer-Emmett-Teller method)
 S_{ext} =external surface area by t-method
 V_{mic} =micropore volume by t-method
 V_{tot} =specific total pore volume
 D_{ave} = Average pore diameter($4V/S_{\text{BET}}$)
 $D_{\text{BJH Ad}}$ =Average pore diameter by BJH method on adsorption branch (cage diameter).
 $D_{\text{BJH De}}$ =Average pore diameter by BJH method on desorption branch (entrance diameter).

Table S1. Surface properties of ***coc*-(Ni/HMS)@SiO₂** and ***conc*-(Ni/HMS)@SiO₂** measured by N₂ adsorption-desorption isotherms at 77 K.

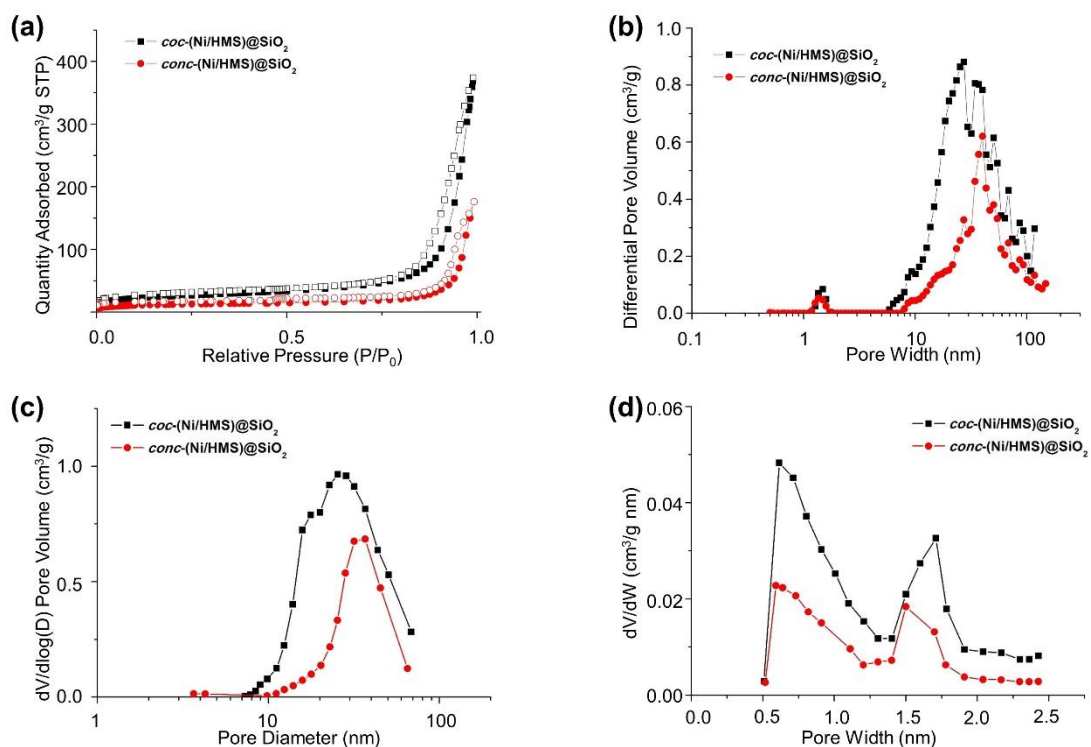


Figure S4. Surface properties measurements and analyses of *conc*-(Ni/HMS)@SiO₂ and *coc*-(Ni/HMS)@SiO₂: N₂ adsorption-desorption isotherms at 77 K (a); pore size distribution obtained by the DFT method, applied to the adsorption branch of the isotherms (b); pore size distribution of the samples obtained by the BJH method on desorption branch (c); pore size distribution (microporous range) obtained by the Horvath Kawazoe(H-K) method (d).

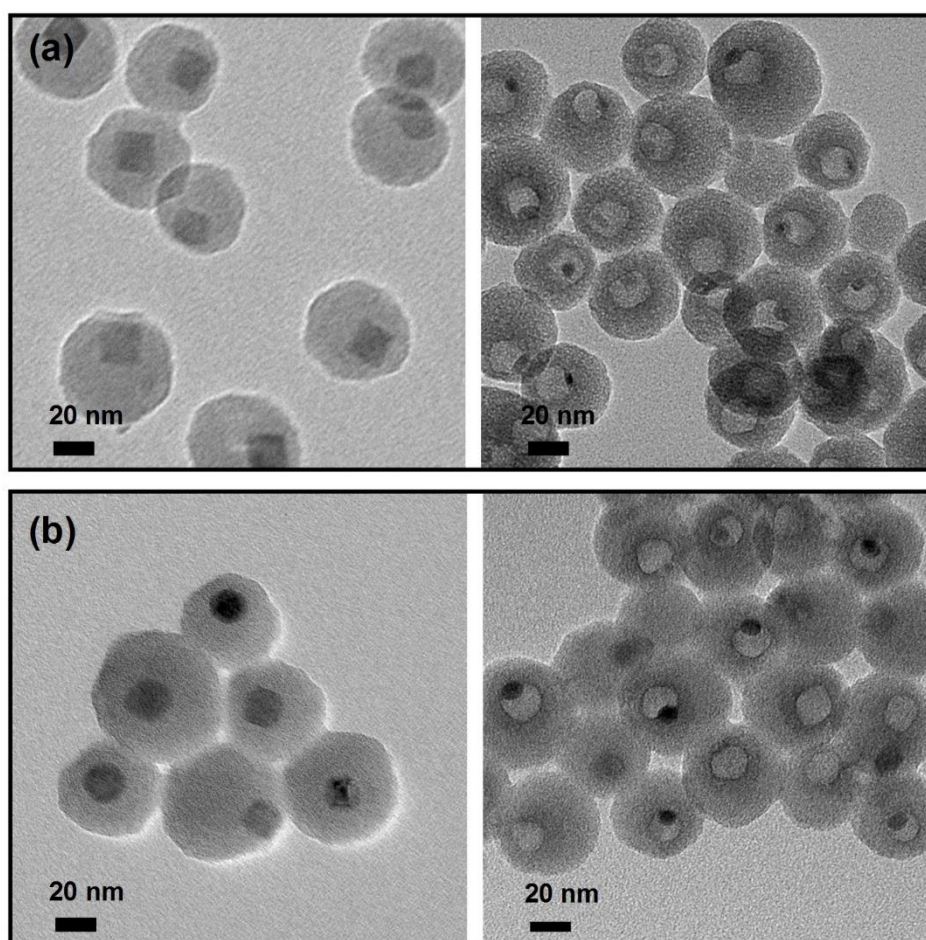


Figure S5. (a) TEM images of *asy*-MnO@(SiO₂/Co²⁺) (left) and *conc*-(Co/HMS)@SiO₂ (right). (b) TEM images of *asy*-MnO@(SiO₂/Cu²⁺) (left) and *conc*-(Cu/HMS)@SiO₂.

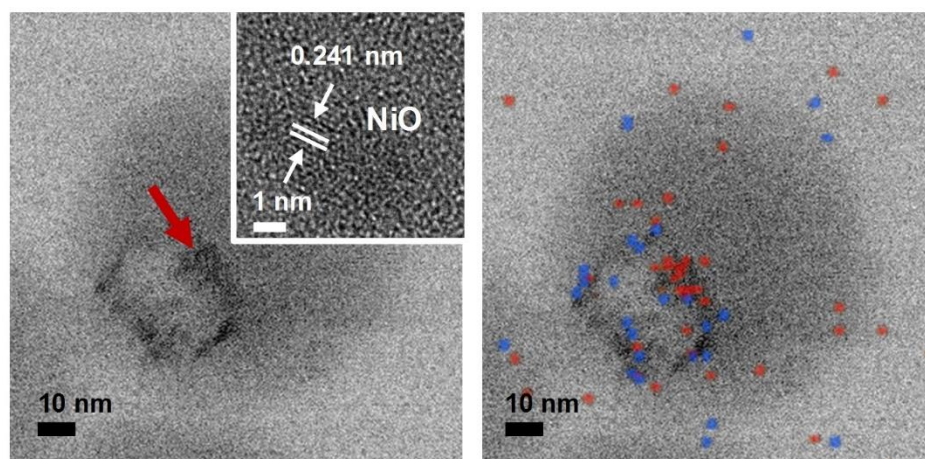


Figure S6. TEM image and HRTEM image (inset) of show state of Ni nanoparticle during galvanic replacement reaction on *conc*-(Ni/HMS)@SiO₂ after 1 hour, right TEM image show EDS mapping of Pt (blue) and Ni (red).

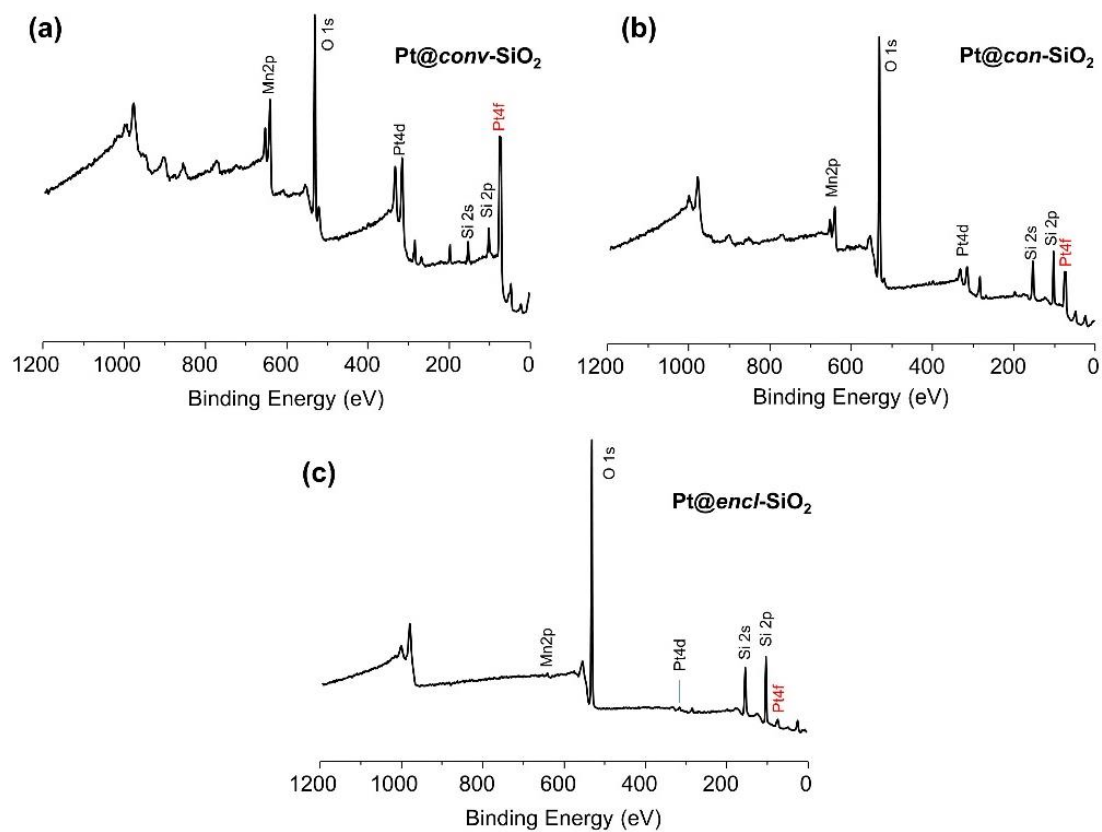


Figure S7. XPS survey spectra of **Pt@con-SiO₂**, **Pt@encl-SiO₂** and **Pt@conv-SiO₂**.

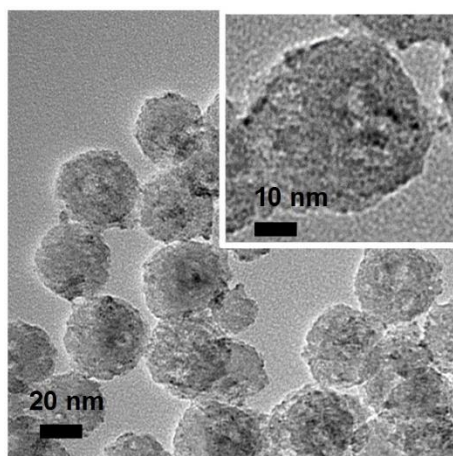


Figure S8. TEM image obtained after galvanic replacement reaction performed on *conc*-(Ni/HMS)@SiO₂ at room temperature and at lower pH condition after 24 h, showing sparse formaton of Pt NCs.

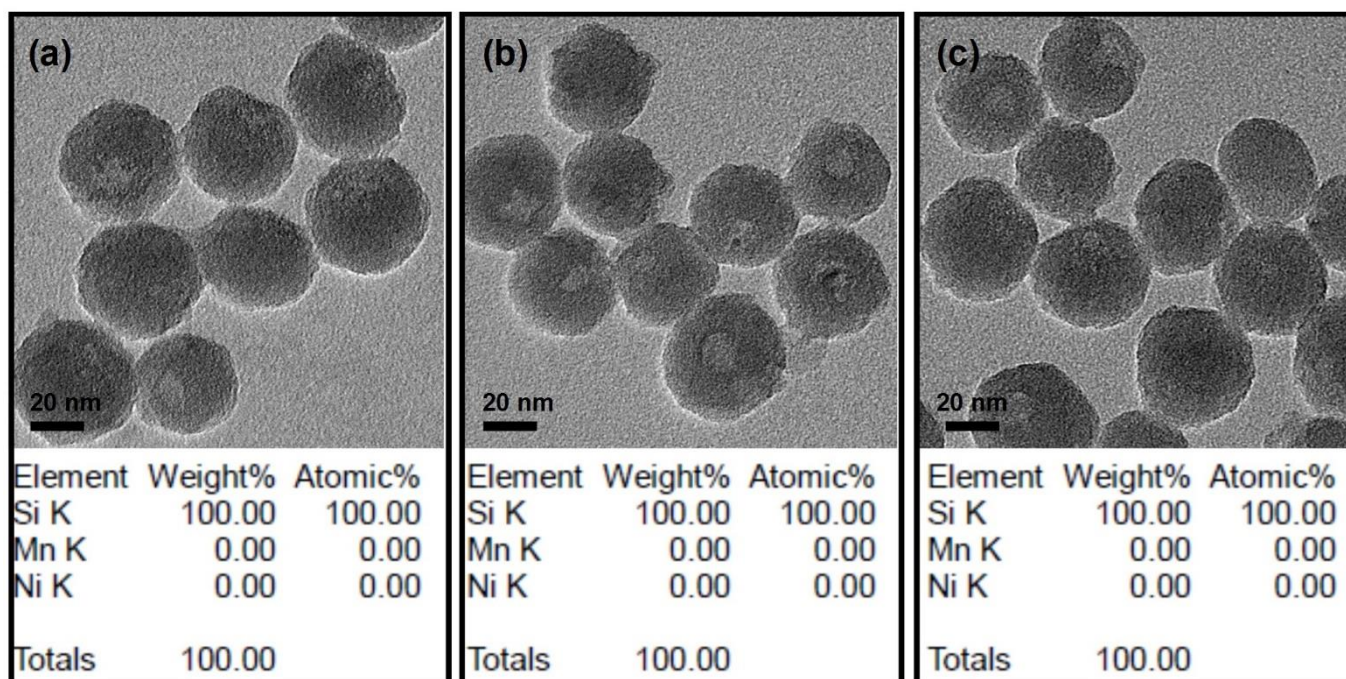


Figure S9. TEM images and EDS data of (a) Mn-free *conc*-(Ni/HMS)@SiO₂ and (b) Mn-free *conc*-(Ni/HMS)@SiO₂ after treatment with Na₂PtCl₄ solution for 2 h and (c) Mn-free *conc*-(Ni/HMS)@SiO₂ after treatment with Na₂PtCl₄/MnCl₂ mixed solution for 2 h.

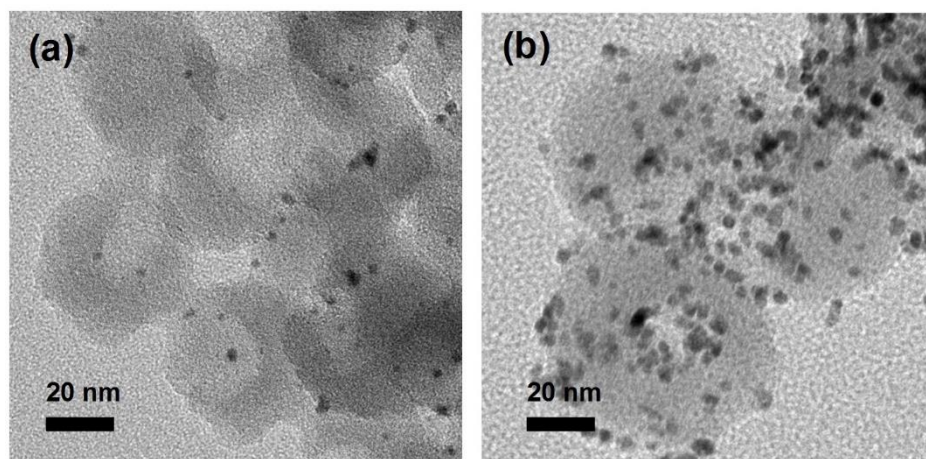


Figure S10. TEM images of (a) Mn-free *conc*-(Ni/HMS)@SiO₂ after treated with Na₂PtCl₄ solution and reducing agent of NaBH₄ at rt for 15 min and (b) Mn-free *conc*-(Ni/HMS)@SiO₂ after treated with Na₂PtCl₄ and reducing agent ethylene glycol at 100 °C for 15 h.

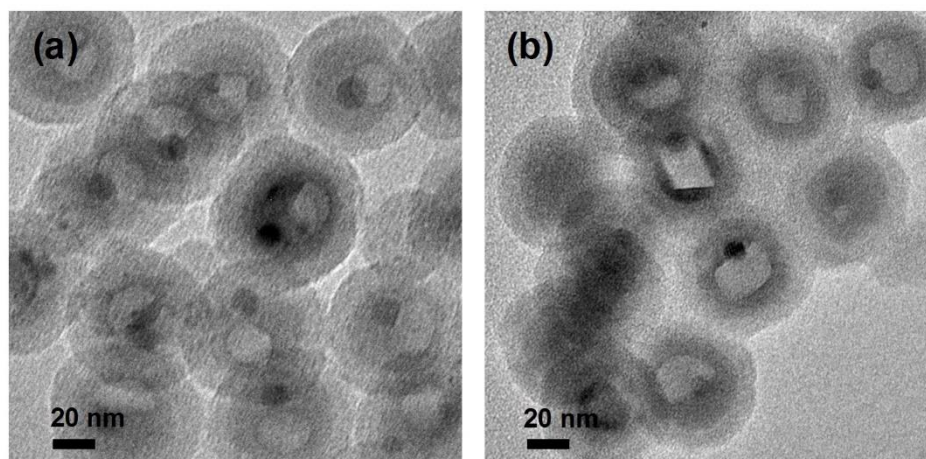


Figure S11. TEM images of (a) *coc*-(Ni/HMS)@SiO₂, (b) after treatment with Na₂PtCl₄ solution at 50 °C for 2 h.

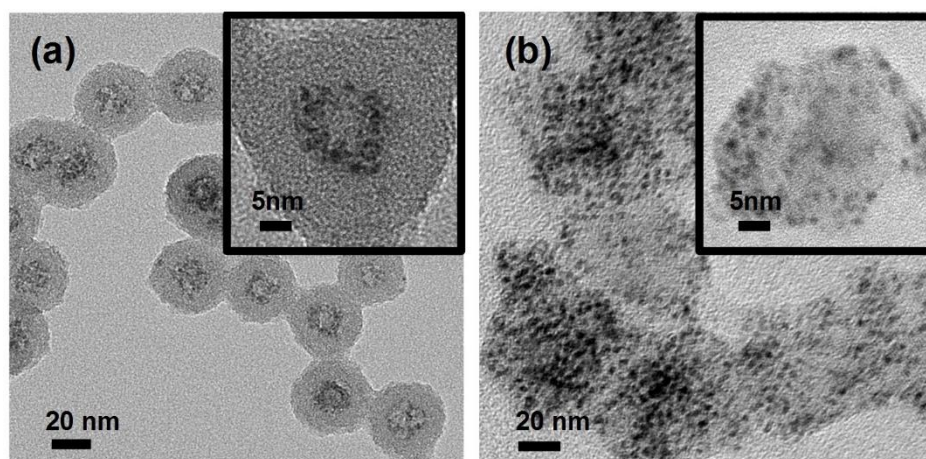


Figure S12. TEM images of (a) **Pt@*encl*-SiO₂** and (b) **Pt@*conv*-SiO₂**

Catalysts	BET specific surface area (m ² g ⁻¹)	specific total pore volume (cm ³ g ⁻¹)	DFT micropore size (nm)	DFT mesopore size (nm)
Pt@<i>conc</i>-SiO₂	123.7	0.43	1.36	34.3
Pt@<i>conv</i>-SiO₂	267.9	0.69	1.36	27.3
Pt@<i>encl</i>-SiO₂	347.0	0.74	1.36	27.3

Table S2. Textural properties of the three catalysts.

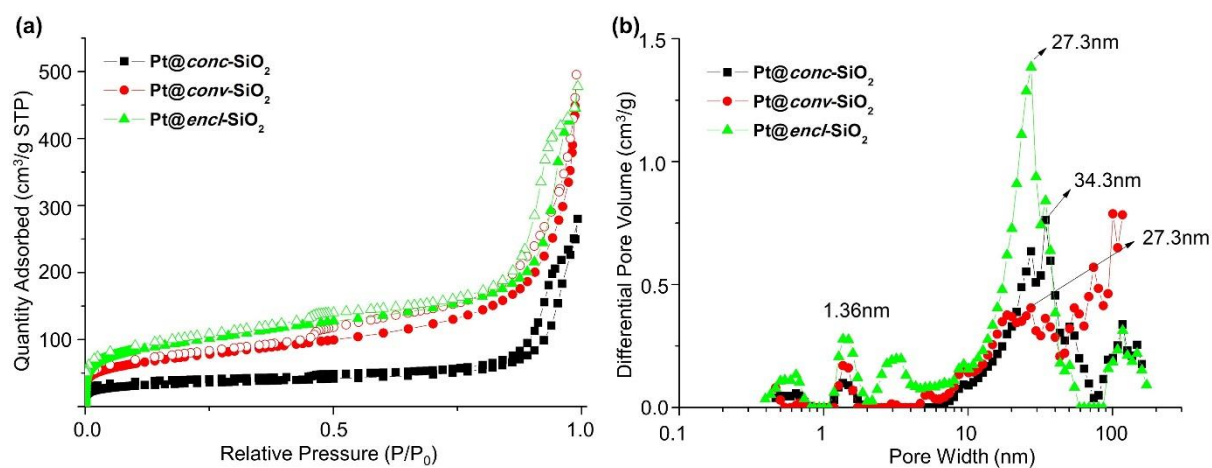


Figure S13. (a) N_2 adsorption-desorption isotherms of the catalysts at 77 K. (b) Pore size distribution of Pt@conc-SiO_2 , Pt@encl-SiO_2 and Pt@conv-SiO_2 obtained by the DFT method, applied to the adsorption branch of the isotherms (left).

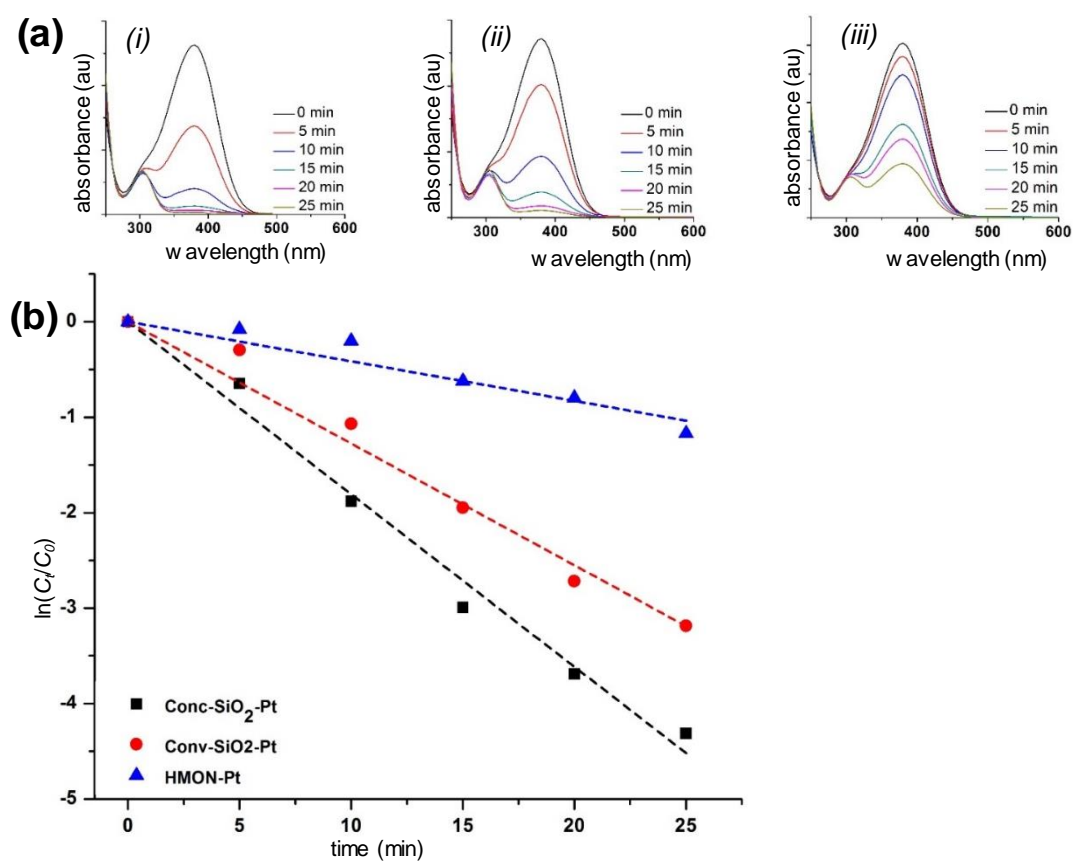


Figure S14. (a) Time-dependent UV-Vis spectra for the reduction of 4-nitroaniline using **Pt@*conc*-SiO₂** (i), **Pt@*conv*-SiO₂** (ii), **Pt@*encl*-SiO₂** (iii). (b) Plots of $\ln(C_t/C_0)$ vs reaction time using different catalysts.

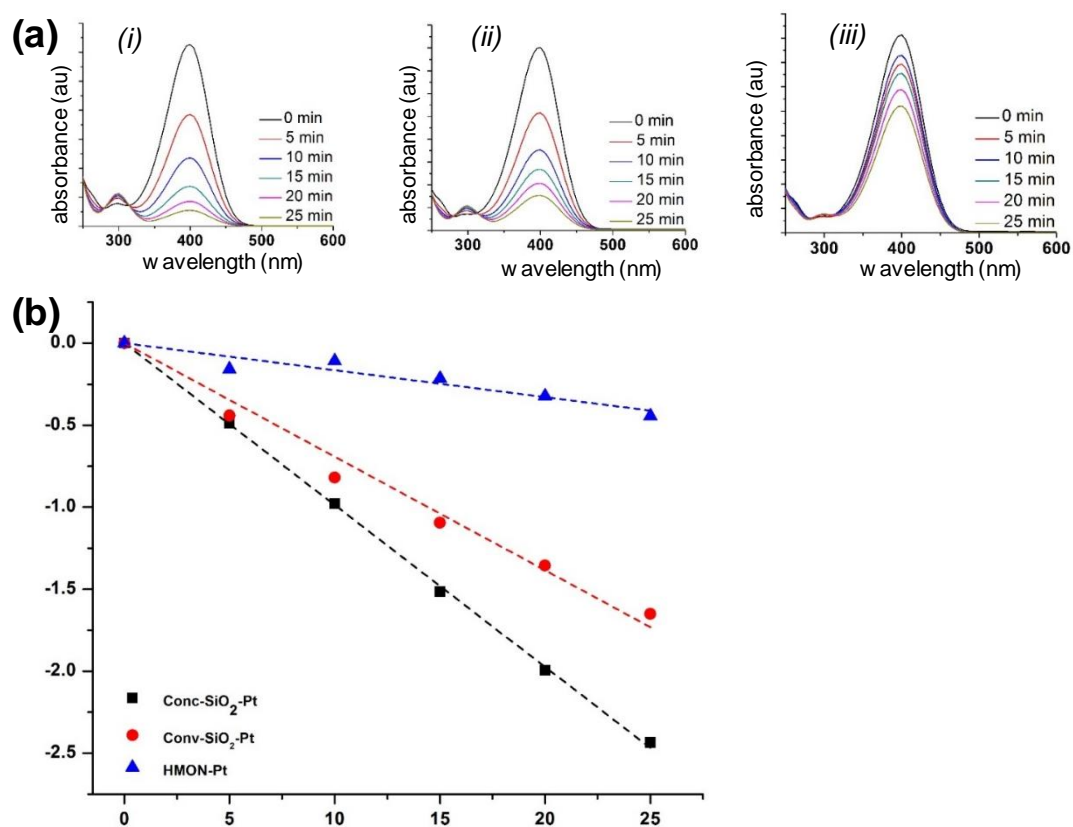


Figure S15. (a) Time-dependent UV-Vis spectra for the reduction of 4-nitrophenol using **Pt@*conc*-SiO₂** (i), **Pt@*conv*-SiO₂** (ii), **Pt@*encl*-SiO₂** (iii). (b) Plots of $\ln(C_t/C_0)$ vs reaction time using different catalysts.

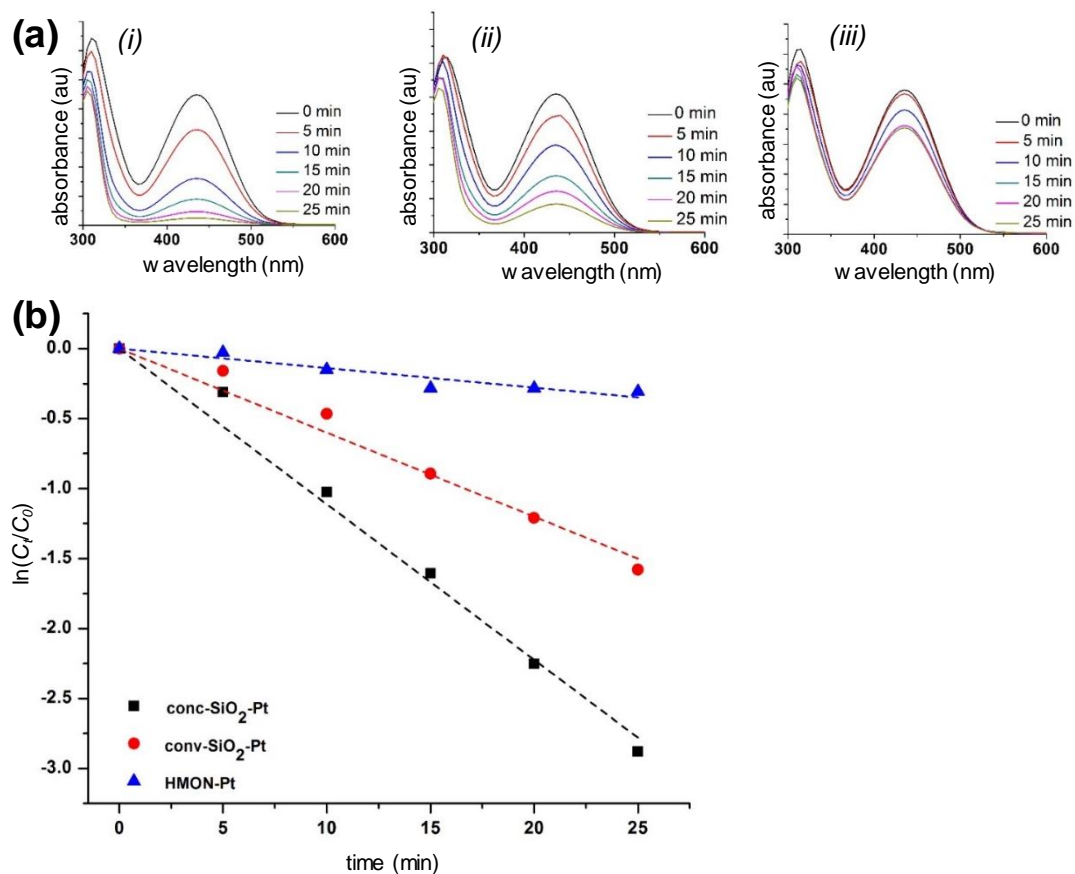


Figure S16. (a) Time-dependent UV-Vis spectra for the reduction of 4'-Amino-5'-nitrobenzo-15-crown-5 using **Pt@conc-SiO₂** (i), **Pt@conv-SiO₂** (ii), **Pt@encl-SiO₂** (iii). (b) Plots of $\ln(C_t/C_0)$ vs reaction time using different catalysts.

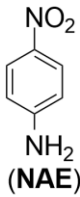
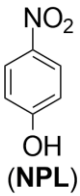
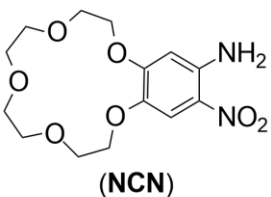
Substrate	Pt@ <i>conc</i> -SiO ₂		Pt@ <i>conv</i> -SiO ₂		Pt@ <i>encl</i> -SiO ₂	
	TON	TOF ₅ (min ⁻¹)	TON	TOF ₅ (min ⁻¹)	TON	TOF ₅ (min ⁻¹)
 (NAE)	995	95	960	64	660	9
 (NPL)	910	77	810	71	360	20
 (NCN)	950	53	790	30	260	5

Table S3. Estimated TON and TOF values for the reduction of NAE, NPL and NCN using all three catalysts. TON values were obtained from the % conversion of the substrates at 25 min of reaction time using 0.1 mol% of catalyst. TOF₅ value were obtained from the % conversion of the substrates at 5 min of the reaction time.

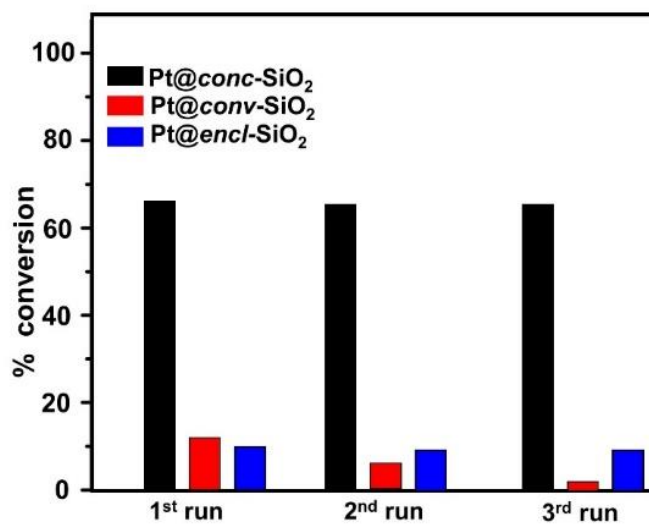


Figure S17. Stability test and comparison of conversion yields (%) for the reduction of 4-nitroaniline using recycled catalysts (0.001 mol%).

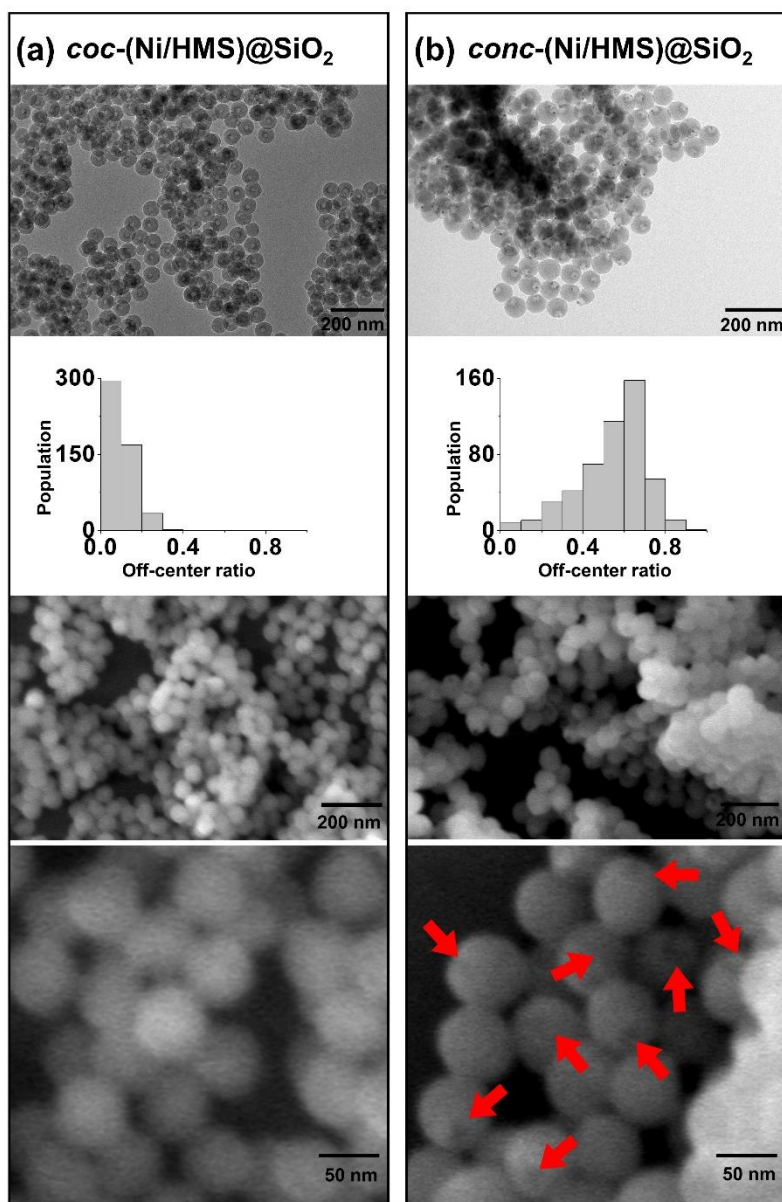


Figure S18. (a-b) Low-magnification TEM, nanoparticle-population-distribution of off-center ratios obtained from TEM images, low magnification SEM and high magnification SEM of *coc*-(Ni/HMS)@SiO₂ and *conc*-(Ni/HMS)@SiO₂. Red arrows designate the visible open-mouthed cavities in SEM images.